International Journal of Engineering

Journal Homepage: www.ije.ir

# Joining Two Dissimilar Metals of Aluminum 5052 to Austenitic Stainless Steel 304 using Ultrasonic Friction Stir Welding

W. S. Abdullah[a], M. Shakeri*[a], M. Habibnia[b]

[a] *Faculty of Mechanical Engineering, Babol Noshirvani University of Technology, Babol, Iran*
[b] *Faculty of Mechanical Engineering, Islamic Azad University, Jouybar Branch, Jouybar, Iran*

*PAPER INFO*

*Paper history:*
Received 8 May 2023
Received in revised form 23 May 2023
Accepted 24 May 2023

*Keywords*:
*Friction Stir Welding*
*Ultrasonic Vibrations*
*Aluminum 5052*
*Austenitic Stainless Steel 304*

*ABSTRACT*

In this research, the joining of aluminum alloy 5052 to austenitic stainless steel 304 was investigated. For this purpose, friction stir welding process was used in two modes with and without ultrasonic vibrations. In order to achieve the best welding quality in terms of mechanical and metallurgical properties, welding parameters such as rotational speed, linear speed and frequency were investigated. The aim of this research is to obtain a sample with the best mechanical and metallurgical properties and the lowest residual stress. As a research innovation and the aim of measuring the values of residual stress created in the samples after the welding operation, the new method of drilling and Digital Image Correlation was used. Finally, by examining the results, it has been determined that ultrasonic vibrations have improved the mechanical and metallurgical properties about 15% to a large extent. In order to evaluate the accuracy of the results related to the residual stress, all the samples were subjected to the central drilling test by installing a strain gauge, and it was found that the error is less than 10% and obtained results were accurate and appropriate.

***doi**: 10.5829/ije.2023.36.08b.09*

## 1. INTRODUCTION

Friction stir welding process is a developed method of friction welding [1]. In this process, due to the friction of a small rotating tool resistant to wear and heat, the necessary heat to change the shape of the material is obtained [2]. This process is a combination of plastic deformation and severe liquefaction of the material in the welding zone. Welding parameters determine the flow pattern of the material and the temperature distribution in the joint area, and as a result, they will have a direct effect on the microstructure of this area [3]. Applying the correct arrangement of these parameters requires accurate knowledge of them, as well as checking the background of researches and conducting trial and error experiments. Habibnia et al. [4] investigated the effect of parameters of rotation speed, weld speed, penetrant depth and tool shoulder diameter on the microstructure and defects created during friction stir welding of 5050 aluminum alloy and 304 stainless steel. Boonchouytan et al. [5] investigated the bonding of 6061 aluminum alloys obtained by semi-solid forming method using friction stir welding method. Liu et al. [6] investigated the effect of welding speed parameter on the mechanical properties of 2219 aluminum alloy. El-sayed et al. [7] evaluated the temperature distribution and residual thermal stresses created by the friction stir welding process of 5083 aluminum sheets at different rotational and linear speeds by threaded and conical cylindrical pins. Hongjun et al. [8] evaluated the fatigue life in friction stir welding of different grades of aluminum. In some researches, in order to improve the conditions of friction stir welding, this process is combined with another process. Thoma et al. [9] investigated the joining of steel to aluminum using the effect of ultrasound in friction stir welding. According to the results, it was found that with the use of ultrasound, the dispersion of steel particles in the welding area has become more uniform. Benfar et al. [10]

*Corresponding Author Email: Shakeri@nit.ac.ir (M. Shakeri)

Please cite this article as: W. S. Abdullah, M. Shakeri, M. Habibnia, Joining Two Dissimilar Metals of Aluminum 5052 to Austenitic Stainless Steel 304 using Ultrasonic Friction Stir Welding, ***International Journal of Engineering, Transactions B: Applications***, Vol. 36, No. 08, (2023), 1489-1501

investigated the effect of using ultrasound in friction stir welding on the corrosion rate. Thoma et al. [11] investigated the benefits of using ultrasound in friction stir welding of non-homogeneous steel-aluminum alloy joints. Hong et al. [12] compared the use of ultrasound in friction stir welding of dissimilar metals. It has been observed that with the use of ultrasound, the amount of intermetallic structure has decreased to a great extent, and this effect has also increased the final strength of the weld. In this research, the feasibility of joining two metals, austenitic stainless steel 304 and aluminum alloy 5052, by means of friction stir welding in a thickness of 3 mm has been investigated. The two metals have high corrosion resistance, and their connection can be used in various industries such as shipbuilding, automotive industries and other industries. By combining these two metals, the properties of both metals can be used. In places where high strength is required from steel and in cases where light weight is required, aluminum alloys can be used [4]. Today, making parts with different materials with the aim of improving efficiency is an interesting idea in the engineering industry [13]. The connection of aluminum alloy to steel has many problems due to different mechanical and thermal properties, including a large difference in melting temperature [4]. To connect these two metals, many methods such as melting and non-melting welding are used. There are many problems in melting methods due to differences in melting temperature and other properties. Among these problems, we can mention the creation of intermetallic compounds and rapid cooling, which causes the weld area to become brittle. Also, in the connection by melting methods, the chromium in steel, which is one of the reasons for its resistance to corrosion, turns into chromium carbide and reduces the corrosion resistance [14]. As an innovation in this research, the friction stir welding method using ultrasonic effect has been used to connect these two non-homogeneous aluminum alloy 5052 to austenitic stainless steel 304. The next innovation is the way of measuring the values of residual stress created in the samples after the welding operation, and this is new method of drilling and Digital Image Correlation.

## 2. EXPERIMENTAL WORK

In this research, the friction stir welding process has been performed on cold rolled sheets of aluminum 5052 and austenitic stainless steel 304 with a thickness of 3 mm. The samples are cut by guillotine in dimensions of 100×150 mm and are milled to make the joint edge parallel and flat. Also, before the test, the edge required for the test is cleaned with a file and the oxides are removed. According to Figure 1, after preparing the samples, pictures related to the microstructure were taken from the surfaces of the aluminum and steel samples. Fixtures are used for clamping parts and also for correct positioning. The surface of the fixture is ground so that the penetration depth remains constant in all welding points. For the tool to move correctly on the connecting line and not to deviate, two holes are created at both ends of the plate parallel to the horizontal axis of the device. A line is drawn between these two holes. Two steel and aluminum pieces are placed face to face on this line and are secured by two machined and perforated blocks that are placed on the plate. The fixture plate is connected to the table of the milling machine by means of two T-shaped numbers. To determine the chemical composition percentage of these alloys, a material analysis device (spectrometry) has been used. The chemical composition of austenitic stainless steel 304 and aluminum 5052 are shown in Tables 1 and 2.

To perform the friction stir welding process, two rotary and linear movements of the tool are needed. To provide these two movements, a vertical milling machine


**Figure 1.** Microstructure of (a) steel 304 (b) aluminum 5052 at scale 40x

**TABLE 1.** Chemical composition of aluminum 5052

| Elements (%) | Cr | Al | Other | V | Si | Mn | Mg | Fe | Cu |
|---|---|---|---|---|---|---|---|---|---|
| **Aluminum 5052** | 0.030 | 0.314 | 8.100 | 0.020 | 18.000 | 0.003< | 0025 | 1.090 | 0.490 |

**TABLE 2.** Chemical composition of austenitic stainless steel 304

| Elements (%) | C | Other | Ni | Mo | Cr | S | P | Mn | Si | Fe |
|---|---|---|---|---|---|---|---|---|---|---|
| **Stainless steel 304** | 0.030 | 0.314 | 8.100 | 0.020 | 18.000 | 0.003< | 0.025 | 1.090 | 0.490 | 73.930 |

made by Tabriz Machinery has been used. The rotational speed range of this machine is 45-1500 rpm and the linear speed of the table is 28-900 mm/min. The friction stir welding tool has a decisive role in the quality of the connection. To obtain an acceptable connection, one of the important parameters is the tool wear factor. In the connection of these two metals, in order to minimize the amount of tool wear, tungsten carbide tools with the specifications presented in Table 3 have been used. Machining of this material by lathe and milling machine is not possible due to its high hardness. Grinding machining technique is used to make tools. The tool used to machine this type of material is CBN. The schematic drawing of the tool used in this research is shown in Figure 2.

A milling machine and a fixture are commonly used to perform the friction stir welding process. But to do the test using ultrasound, a set has been designed and built that can create vibration with the desired frequency and amplitude during the process. An ultrasound machine consists of four main parts. The first part is the power supply, which is responsible for changing the frequency from 50 Hz to 20-30 kHz. The next part is the transducer, which performs the task of converting electrical frequency to mechanical frequency. The third part is the signal amplifier and the last part is the horn, which is responsible for transmitting the vibration. All the above items should be placed on a structure and also a fixture for welding should be designed and built. A view of this collection is shown in Figure 3.

According to the vibration direction and amplitude, this set should be designed and built to be installed on the vertical milling machine. In order to investigate the effect of ultrasound on the obtained results, the results will be compared with conventional friction stir welding without vibration. Many parameters are effective in achieving better efficiency in welding quality. In this research, some welding parameters, line frequency of vibration, feed rate and rotational speed are investigated. The investigated parameters and their levels are shown in Table 4.

In order to investigate the effect of each parameter, full factorial design of experiment was conducted. According to the examined parameters, 27 tests should be performed, which are done in form.

**TABLE 3.** Specifications of the tools used

| Pin shape | Shoulder shape | Pin diameter (mm) | concavity angle (degree) | Pin height (mm) | Shoulder diameter (mm) |
|---|---|---|---|---|---|
| Cylinder | Cylinder | 6 | 3 | 2.8 | 20 |

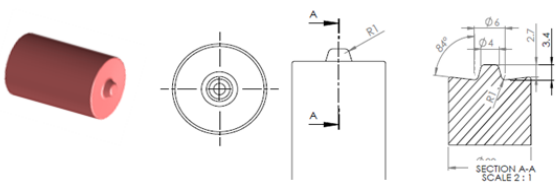

**Figure 2.** Friction stir welding tool

## 3. RESULTS AND DISCUSSION

In order to investigate the effect of input parameters on the connection area, mechanical and metallurgical tests were used, each of these tests was performed according to the desired standard.

**3. 1. Tensile Test** To investigate the tensile behavior of the parts resulting from the friction stir welding process, samples from the welded area were prepared and subjected to tension. Using the results of the tensile test, useful information can be obtained about the ultimate strength, percentage of elongation and toughness. In this research, tensile test samples were prepared based on ASTM E8 standard. The schematic of standard sample is shown in Figure 4 and the samples prepared for the tensile test are shown in Figure 5.

**TABLE 4.** The levels of the investigated parameters

| Frequency (KHz) | Welding speed (mm/min) | Rotational speed (RPM) |
|---|---|---|
| 15 | 28 | 600 |
| 20 | 40 | 800 |
| 25 | 60 | 1000 |

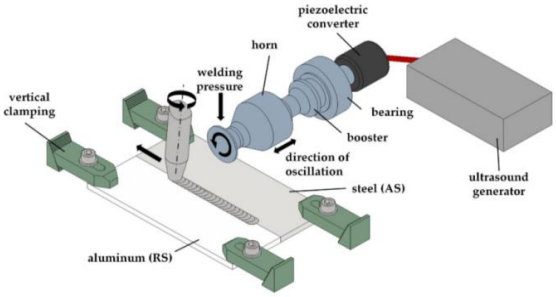


**Figure 3.** Ultrasonic friction stir welding equipment

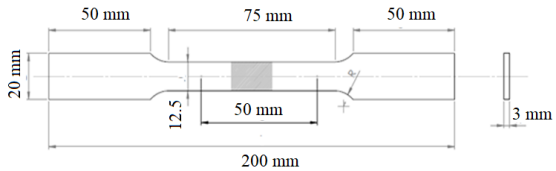


**Figure 4.** Dimensions of tensile test sample according to ASTM E8 standard

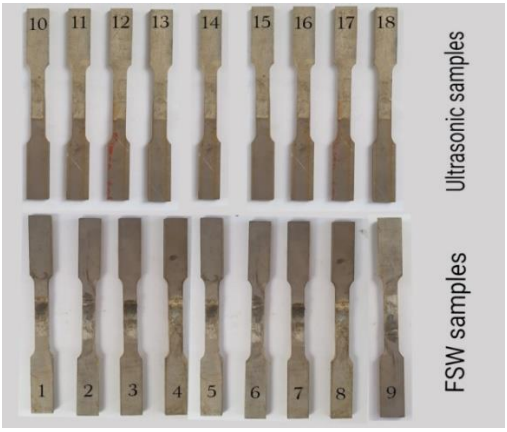


**Figure 5.** Prepared samples for welding

After preparing the samples, all of them were subjected to a tensile test and stretched until breaking. The samples welded by the usual friction stir welding process and with ultrasonic vibrations are shown in Figure 6. According to the tensile test results, it has been determined that the samples subjected to welding with ultrasonic vibrations have better mechanical properties than the samples with friction stir welding normally. During the friction stir welding process, due to the vibration of the work piece, the materials in the stir area get more strain than the same materials in the friction stir welding process. According to the researches, there is a direct relationship between the strain and the density of dislocations in the strained material. It is predicted that the density of dislocations in the stir zone of the vibrating friction welding part is more than its number in the other stir zone of the welded part, and therefore, during the dynamic recrystallization process, more high-angle boundaries are formed and the welding zone formed with a smaller grain size. Tensile test diagram of a sample without vibration and with vibration after the tensile test is shown in Figure 7. According to Figure 7, it has been determined that the sample welded by ultrasonic friction stir method has a higher ultimate tensile strength and elongation percentage than the friction stir welding sample. The reason for this can be the smaller grain size of the friction stir welding sample. According to the Hall-Patch relationship, strength has a direct relationship with the inverse of the square of the grain size, and the strength will increase as the grain size decreases. In fact, with the reduction of the grain size, the volume component of the grain boundaries will increase, and since the grain boundaries act as an obstacle against the movement of dislocations, the strength decreases with the reduction of the grain size. According to the mentioned cases, it can be seen that by performing ultrasonic friction stir welding and reducing the grain size in the stir zone, since the mechanical properties of the stir zone are improved. Therefore, the strength and the elongation percentage of the welded sample will also increase.

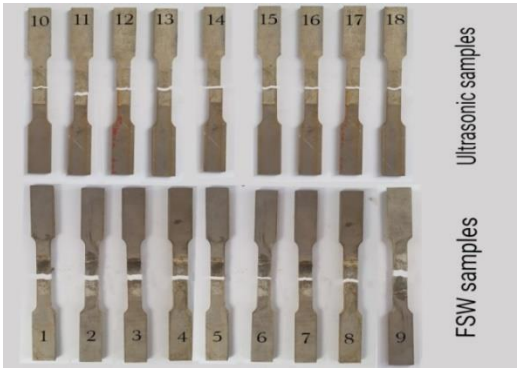


**Figure 6.** Welded samples after tensile test

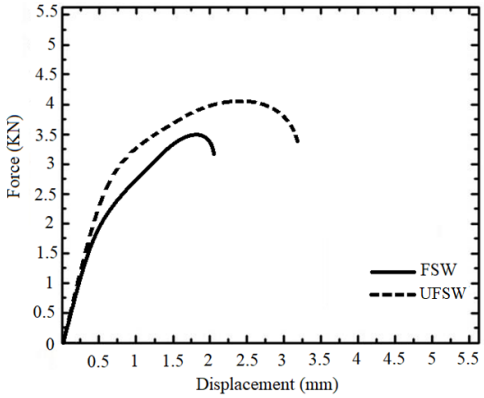


**Figure 7.** Force-displacement diagram of friction stir welding process and ultrasonic friction stir welding process

Although most of the conducted researches emphasize the reduction of grain size and its effect on increasing strength, there is no common opinion regarding the changes in elongation in the tensile test in terms of grain size changes. According to Figure 7, it is clear that with the reduction of the grain size in the welding area, the percentage of elongation has increased. The reason for this can be attributed to the increase in the number of boundary dislocations with the increase in the volume component of the grain boundaries and the other issue is the further prevention of grain boundaries from crack growth in fine-grained materials. Grain boundaries are the place of accumulation of geometrically essential dislocations. Since the possibility of plastic deformation increases with an increase in the number of dislocations, it is predicted that the length change due to tension will increase with the decrease in the grain size, also the results of the investigations have shown that with the decrease in the size due to the change of the fracture mechanism from grain boundary to multigrain, the elongation percentage increases. The value of welded samples maximum force using the ultrasonic friction stir method is shown in Figure 8.

In general, it can be seen that with the increase in frequency, the strength of the parts and the percentage of

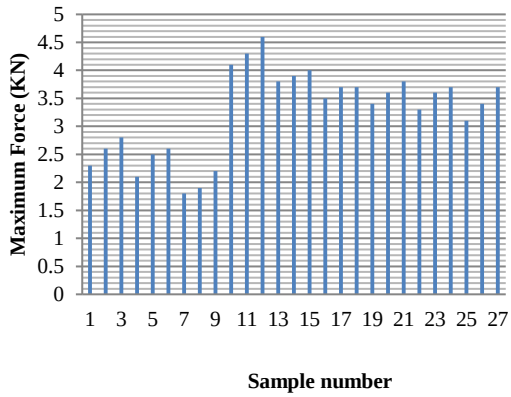


**Figure 8.** The values of the maximum force applied to friction stir welding samples

length increase have also increased. The reason for this can be attributed to the effect of vibration. By increasing the vibration frequency, the strain rate increases during the friction stir welding process and more dislocations are produced during welding. Since the main mechanism for fineness in the friction stir welding process is dynamic recrystallization, with an increase in the production of dislocations, more recrystallization takes place and as a result, the microstructure with smaller grains is obtained. This issue can also be interpreted using the Zener-Holoman variable. As the strain increases according to Equation (1), the value of the Zener-Holman variable (Z) increases.

$$Z=\dot{\varepsilon}.\exp(\frac{Q}{RT}) \quad (1)$$

In Equation (1), $\dot{\varepsilon}$ is the strain rate, T is the working temperature in degrees Kelvin, Q is the activation energy, and R is the gas constant. The relationship between the parameter Z and the average size of sub-grains or dynamically crystallized grains follows the relation D-1=aLnZ-b. In such a way that D is the average size of grains, Z is the Zener-Lonman parameter, and a and b are positive numbers. By increasing the variable Z according to Equation (1), the grain size decreases and as a result, according to the Hall-Patch relation, the strength value increases.

**3. 2. Microhardness Measurement** To study the effects of friction stir welding on the hardness of the samples and check the hardness changes in different areas, after welding, the sheets were cut perpendicular to the process direction and molded and mounted with a special resin solution. Due to the very low force in the microhardness test and its small effect on the welding surface, the surface of the samples should be polished well before the test. To do this, the samples are rasped by carbide rasping sheets up to 1500 series. To study the macrostructure of friction stir welding samples, the sheets are cut and mounted in the direction perpendicular to the process. The mounted samples are first rasped by carbide rasping sheets up to 5000 series and then polished by $Al_2O_3$ powder. An optical microscope has been used to investigate the distribution of steel particles in the disturbed area and also to see defects such as holes and cracks. In joining two metals of aluminum alloy to stainless steel, there is a possibility of creating intermetallic structures, X-ray spectroscopy is used to identify these intermetallic structures. In this method, by measuring the Bragg angle (α2) and the distance between the crystal plates, the compounds in the desired area can be obtained.

According to the investigations, the hardness value in the stir area has increased for all the samples, and its value will decrease by moving towards the two base metals. The hardness value for 304 steel base metal is around 210 HV and for 5052 aluminum around 80 HV. By moving from the side of the base metals to the stir zone, the hardness values have increased. Hardness profile for a welded sample is shown in Figure 9. Research shows that the change of hardness in friction stir welding for aluminum alloys that have the ability to be heat treated is different from the alloys without the ability to be heat treated. In friction stir welding for some heat treatable aluminum alloys, the middle region of the welded section has less hardness than other regions. Hardness values of the samples after friction stir welding are shown in Tables 5 and 6. According to the investigations, it has been determined that at a constant weld speed, the hardness value in the stir area has decreased as average of 25% with an increase in the rotational speed of the tool.

Relation between all parameters and their effects on each other is considerable. ANOVA analysis for selected factorial is shown in Table 7.

The Model F-value of 90.63 implies the model is significant. There is only a 0.01% chance that an F-value this large could occur due to noise. P-values less than 0.05 indicate model terms are significant. In this case A, B, C, AB are significant model terms. Values greater than0.10 indicate the model terms are not significant. If there are many insignificant model terms (not counting those required to support hierarchy), model reduction

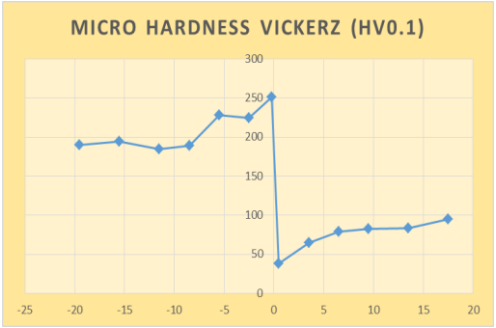


**Figure 9.** Micro hardness profile of sample 1

**TABLE 5.** Hardness values of sample 1 welded by ultrasonic friction stir method

| **Distance from weld center (mm)** | **-8 (base metal of steel area)** | -5 | -4 | -3 | -2 | -1 |
|---|---|---|---|---|---|---|
| **Hardness (HV)** | 200 | 230 | 226 | 224 | 242 | 247 |
| **Distance from weld center (mm)** | 0 | 1 | 2 | 3 | 4 | **8 (base metal of aluminum area)** |
| **Hardness (HV)** | 250 | 45 | 49 | 62 | 68 | 81 |

**TABLE 6.** Hardness values of the welded samples by the ultrasonic friction stir method

| **Sample number** | **Hardness in aluminum zone (HV)** | **Hardness in steel zone (HV)** |
|---|---|---|
| 1 | 68 | 242 |
| 2 | 63 | 229 |
| 3 | 59 | 220 |
| 4 | 73 | 256 |
| 5 | 71 | 248 |
| 6 | 66 | 245 |
| 7 | 80 | 268 |
| 8 | 72 | 258 |
| 9 | 70 | 252 |
| 10 | 52 | 231 |
| 11 | 50 | 222 |
| 12 | 45 | 213 |
| 13 | 64 | 239 |
| 14 | 64 | 231 |
| 15 | 57 | 223 |
| 16 | 70 | 249 |
| 17 | 63 | 241 |
| 18 | 59 | 234 |
| 19 | 47 | 222 |
| 20 | 43 | 212 |
| 21 | 40 | 203 |
| 22 | 56 | 234 |
| 23 | 52 | 232 |
| 24 | 49 | 221 |
| 25 | 62 | 248 |
| 26 | 58 | 246 |
| 27 | 55 | 229 |

**TABLE 7.** ANOVA for selected factorial

| **Source** | **Sum of Squares** | **df** | **Mean Square** | **F-value** | **p-value** | |
|---|---|---|---|---|---|---|
| **Model** | 2513.26 | 10 | 251.33 | 90.63 | < 0.0001 | **significant** |
| **A-Rotational speed** | 1316.07 | 2 | 658.04 | 237.29 | < 0.0001 | |
| **B-Welding speed** | 848.30 | 2 | 424.15 | 152.95 | < 0.0001 | |
| **C-Frequency** | 291.63 | 2 | 145.81 | 52.58 | < 0.0001 | |
| **BC** | 57.26 | 4 | 14.31 | 5.16 | 0.0073 | |
| **Residual** | 44.37 | 16 | 2.77 | | | |
| **Cor Total** | 2557.63 | 26 | | | | |

may improve your model. Relation between parameters and their effects on hardness at different frequencies is shown in Figures 10-12.

Microstructure of the weld zone of the sample welded by ultrasonic friction stir process is shown in Figure 13. According to the images related to the microstructure, it has been determined that with the increase in the linear speed of the tool, the grain size in the welding area has decreased, and with an increase in the rotational speed of the tool, the grain size in the welding area has increased. Based on the researches, it has been determined that by increasing the rotation speed of the tool and decreasing the linear speed, more heat will be generated in the

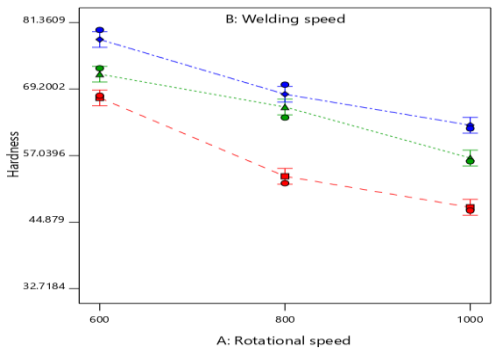


**Figure 10.** Relation between parameters at frequency 15KHz

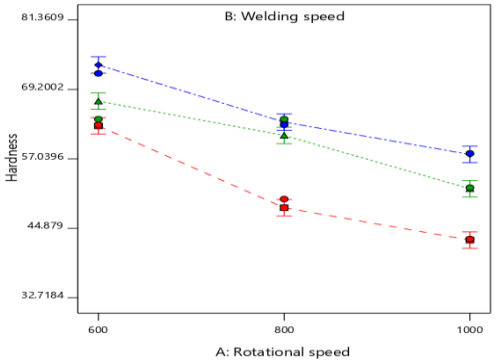


**Figure 11.** Relation between parameters at frequency 20KHz

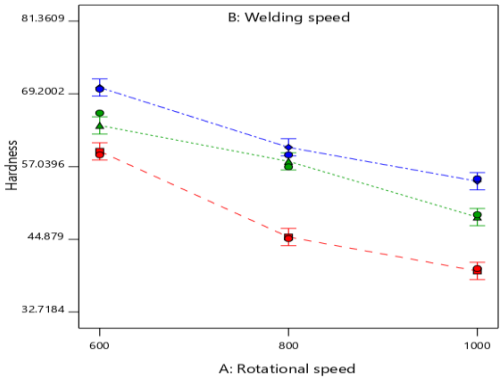


**Figure 12.** Relation between parameters at frequency 25KHz

welding area during the welding operation. The high heat generated in the friction stir welding process will cause grain size growth in the weld zone.

According to Figure 13, it is clear that the mixing operation between steel and aluminum has been done well and the particles are observed in fine form in each other's structure. There are no visible defects, holes, and cracks, and in the aluminum nugget, the grains have elongation, which actually have flowed.

**3. 3. Residual Stress** Residual stress is the stress that will still exist in the part after loading. This tension is beneficial in some parts and harmful in some parts [15].


**Figure 13.** Microstructure of the aluminum-steel joint at scale 10x

There are different methods for measuring residual stress, and in this research, the method of Digital Image Correlation (DIC)-Central Hole Drilling is used. In the method of DIC, first, a random black and white speckle pattern is created on the surface of the part. After preparing the sample, before and after loading, two pictures of the speckle pattern of the part surface are taken, and then by analyzing these two pictures in the correlation algorithm, the field of displacement and strain can be obtained. A schematic of the DIC method equipment is shown in Figure 14. The main idea of this method is how to establish a connection between the points before and after the change of shape in the examined material. The method of DIC does this by using sub-parts of the reference photo, which are known as subsets, and determines their relative position. For each subset, displacement and strain information is calculated during the transfer to match the position of the subsets in the current condition. The final result of a network includes displacement and strain information according to the reference configuration information. In the method of DIC, the light intensity of each photo is estimated with a continuous polynomial function. Sutton et al. [16] showed in an article that the 5th degree curve shows the best results. Each time, the mapping algorithm compares the light intensity function of two subsets of two images before and after loading with dimensions of N×N pixels, and selects that subset of the photo after loading, which has the most agreement with the subset of the reference photo, as the subset of change. It considers the finding and obtains its displacement and deformations (according to Figure 15). This process is done for all the subsets of the reference image and finally the total displacement field is obtained. In order to check the degree of conformity of each pair of subsets, the correlation coefficient C is defined as Equation (2), which can be a suitable criterion for understanding the degree of conformity of two corresponding subsets [16].

$$C(R)=\frac{\sum_{i=-m}^{i=m}\sum_{j=-m}^{j=m}\left(G_r\left(X_p,Y_p\right)-G_d\left(X_p^{'},Y_p^{'}\right)\right)^2}{\sum_{i=-m}^{i=m}\sum_{j=-m}^{j=m}\left(G_r\left(X_p,Y_p\right)\right)^2} \quad (2)$$

Which in Equation (2):

$$X_p = x_p + i$$

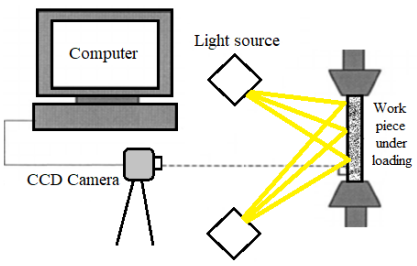


**Figure 14.** Schematic of the DIC process

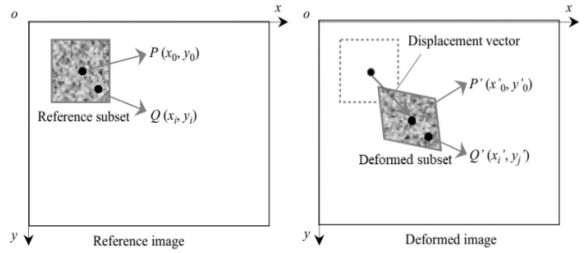


**Figure 15.** Reference and deformed subsets

$$Y_p = y_p + j$$

$$X_p^{'} = x_p + i + U_s(i,j)$$

$$Y_p^{'} = y_p + j + V_s(i,j)$$

And R is the unknown vector as follows:

$$R = (X, Y, U, V, \frac{\partial u}{\partial x}, \frac{\partial v}{\partial x}, \frac{\partial u}{\partial y}, \frac{\partial v}{\partial y})$$

In above equations, U and V are displacement components, $G_r$ andare continuous functions of $G_d$ light intensity interpolation before and after loading. $(x, y)$ and $(x', y')$ are points coordinates in subsets of reference and deformed image that relate to each other according to Equations (3) and (4) [16].

$$X' = x + U + \frac{\partial U}{\partial x}\Delta x + \frac{\partial U}{\partial y}\Delta y \quad (3)$$

$$Y' = y + V + \frac{\partial V}{\partial x}\Delta x + \frac{\partial V}{\partial y}\Delta y \quad (4)$$

In Equations (3) and (4), Δx and Δy are horizontal and vertical distances of the point (x, y) from the subset center. In correlation relation, the amount of light intensity at each point of reference image subset is compared with the same subset in the image after loading and their difference is obtained. Then the square of their difference is divided by the square of light intensity of that point in the reference image. The obtained number is a measure of the relative error at that point. To calculate the sum of total error in a subset, the error values of the points are added together, when the correlation coefficient is zero, in fact, the error function in the whole subset is zero, and this indicates a complete match. The best solution is obtained when the coefficient C(R) in Equation (2) is minimized. In other words, interpolation functions are slightly different before and after loading anywhere. According to Equation (5), to minimize C, its gradient must be zero.

$$\nabla C = \left(\frac{\partial C}{\partial R_k}\right)_{k=1,13} \quad (5)$$

The Newton-Raphson method is used to solve the Equation (5) and obtain its roots. This method uses an approximate initial value to find the root of the equations and repeats until the error is less than a certain value. Since the correlation coefficient is a function of the displacement components and their gradients, these unknowns can be obtained by searching for a category of these components that minimize the correlation coefficient. In the correlation method algorithm, the search process for calculating the unknown displacements and displacement gradients is started with long steps. In this process, the displacement gradients are initially considered zero, and the algorithm searches for the 1-pixel steps in interest area and the pixel that minimizes the correlation coefficient is considered as the initial solution. Then, using the Newton-Raphson method, their displacements and gradients are accurately obtained with a fraction of pixel size. The results of this step are used as initial values in the Newton-Raphson algorithm for the next subset [17]. In this method, by performing general calculations, finally, the strains in different directions are calculated as Equations (6)-(8):

$$\varepsilon_{xx} = \frac{1}{2}((\frac{du}{dx})^2 + (\frac{dv}{dx})^2 + (\frac{dw}{dx})^2) + (\frac{du}{dx}) \quad (6)$$

$$\varepsilon_{yy} = \frac{1}{2}((\frac{du}{dy})^2 + (\frac{dv}{dy})^2) + (\frac{dv}{dy}) \quad (7)$$

$$\varepsilon_{zz} = \frac{1}{2}((\frac{du}{dy}) + (\frac{dv}{dx})) + \frac{1}{2}(\frac{du}{dx}\frac{du}{dy} + \frac{dv}{dx}\frac{dv}{dy}) \quad (8)$$

According to Figure 16, in the central hole drilling method, first a rosette strain gauge is attached to the surface of a piece with residual stress. In the Rosette strain gauge, the optimal strain measurement points for the strain gauges have been observed. Then a small hole with a depth slightly larger than the diameter of the hole is created in the center of the rosette strain gauge. This hole locally releases the stresses in the environment around the hole and the released strains are measured by three strain gauges on the rosette.

In this regard, Schajer and Yang [18] defined nine calibration coefficients to relate the residual stress and

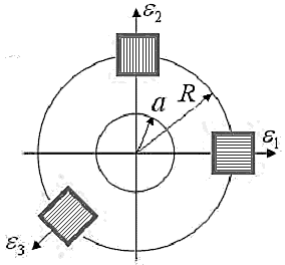


**Figure 16.** Strain gauge installation location in central drilling method

released strain, which can be obtained by theoretical, numerical and experimental methods. With an analytical solution, they calculated the calibration coefficient values for a suitable range of different mechanical properties of orthotropic materials. They used the following matrix relation:

$$\begin{bmatrix} C_{11} & C_{12} & C_{13} \\ C_{21} & C_{22} & C_{23} \\ C_{31} & C_{32} & C_{33} \end{bmatrix} \begin{bmatrix} \sigma_x \\ \sigma_y \\ \sigma_{xy} \end{bmatrix} = \begin{bmatrix} \varepsilon_1 \\ \varepsilon_2 \\ \varepsilon_3 \end{bmatrix} \quad (9)$$

In Equation (9), the softness or calibration coefficients $C_{11}$ to $C_{33}$ depend on the elastic properties of the sample, the diameter and depth of the hole and the geometry of the strain gauge. In order to calculate these values, it is possible to use the analytical solution [19], referring to the standard and finite element simulation. In this research, reference is made to the standard in order to calculate the calibration coefficients.

Equations (10-18) can be used to measure the stress around the created hole. The strain values must be used to calculate the following constants as shown in Equations (10-12) [20].

$$p = \frac{\varepsilon_3 + \varepsilon_1}{2} \quad (10)$$

$$q = \frac{\varepsilon_3 - \varepsilon_1}{2} \quad (11)$$

$$t = \frac{\varepsilon_3 + \varepsilon_1 - 2\varepsilon_2}{2} \quad (12)$$

As stated, there are different methods for calculating calibration coefficients, and after calculating these coefficients, their values are incorporated in Equations (13-15) [20].

$$P = \frac{\sigma_y + \sigma_x}{2} = -\frac{Ep}{\bar{a}(1+\vartheta)} \quad (13)$$

$$Q = \frac{\sigma_y - \sigma_x}{2} = -\frac{Eq}{\bar{b}} \quad (14)$$

$$T = \tau_{xy} = -\frac{Et}{\bar{b}} \quad (15)$$

After calculating Equations (13-15), the values of plate stresses can be calculated using the Equations (16-18) [20].

$$\sigma_x = P - Q \quad (16)$$

$$\sigma_y = P + Q \quad (17)$$

$$\tau_{xy} = T \quad (18)$$

Equation (19) can also calculate the maximum and minimum stresses. The maximum tensile (or minimum compressive) principal stress, $\sigma_{max}$ is at the angular position β in the clockwise direction relative to the strain gauge position 1 which is shown in the Figure 16. As the same way, minimum tensile (or maximum compressive) principal stress, $\sigma_{min}$ is at the angular position β in the clockwise direction relative to the strain gauge 3 which is shown in the Figure 16. The angle β can be calculated by Equation (20) [20-22].

$$\sigma_{max}, \sigma_{min} = P \pm \sqrt{Q^2 + T^2} \quad (19)$$

$$\beta = \frac{1}{2} arc \tan\left(\frac{-T}{-Q}\right) \quad (20)$$

In Figure 17, the intended device for performing the drilling-DIC is presented.

As mentioned, in order to measure the amount of residual stress in the samples, the target piece is subjected to drilling operation in 10 stages and after each stage of drilling, the surface of the hole is imaged using IC Capture software. In Figure 18, 4 stages of imaging during the drilling operation are shown. After the drilling operation, all the recorded photos will be entered into the image processing software (GOM Correlate) and the

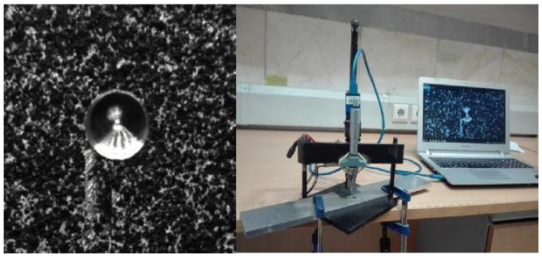

**Figure 17.** The device for residual stress measurement

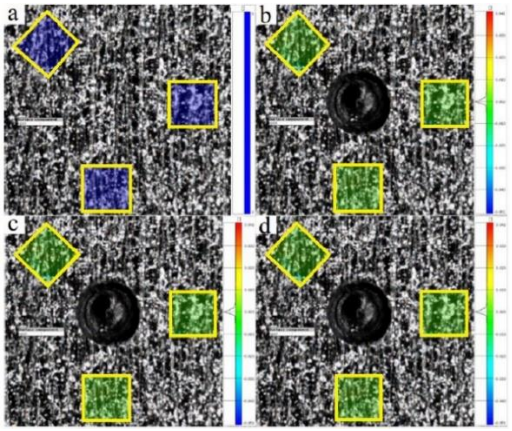


**Figure 18.** Stages of performing drilling operations step by step

desired mesh will be done in the software. An example of the image of the hole created on the sample and the mesh made on it are shown in Figure 19.

After meshing the sample and performing the required operations, at the end, the strain values released on the sample will be extracted numerically and contour. The contour of the strain released around the hole during the central drilling operation is shown in Figure 20. Finally, by checking the released strain values for all samples and using the required relationships, the residual stress values will be calculated. The values of the residual stress in the samples welded by the ultrasonic friction stir welding process are shown in Table 8.

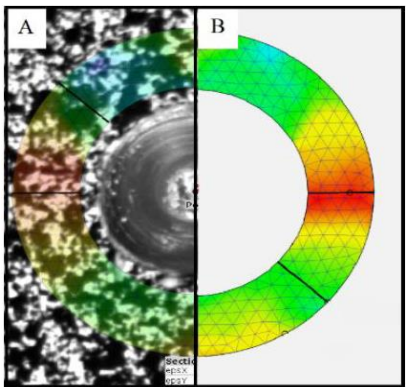


**Figure 19.** Meshing done on the sample image

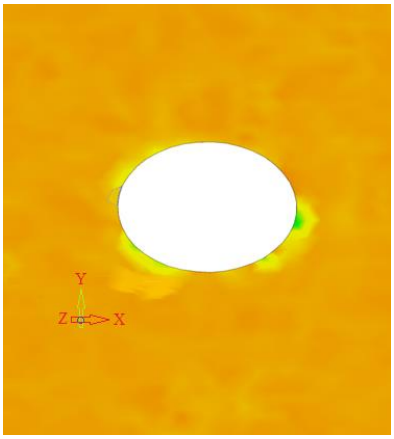


**Figure 20.** The contour of the strains released on the sample after the drilling operation

**TABLE 8.** Residual stress values for all ultrasonic friction stir welding samples

| Sample number | Residual stress in aluminum zone (MPa) | Residual stress in steel zone (MPa) |
|---|---|---|
| 1 | 121 | 323 |
| 2 | 113 | 302 |
| 3 | 106 | 293 |
| 4 | 144 | 336 |
| 5 | 131 | 329 |
| 6 | 120 | 312 |
| 7 | 148 | 353 |
| 8 | 141 | 350 |
| 9 | 129 | 339 |
| 10 | 160 | 366 |
| 11 | 152 | 350 |
| 12 | 141 | 337 |
| 13 | 166 | 380 |
| 14 | 164 | 371 |
| 15 | 164 | 366 |
| 16 | 169 | 384 |
| 17 | 144 | 379 |
| 18 | 138 | 377 |
| 19 | 175 | 395 |
| 20 | 164 | 389 |
| 21 | 148 | 377 |
| 22 | 181 | 406 |
| 23 | 166 | 398 |
| 24 | 152 | 388 |
| 25 | 188 | 425 |
| 26 | 159 | 402 |
| 27 | 153 | 373 |

The residual stress values depend on the thermal gradients created in the samples and their plastic deformation. According to the results, it has been determined that at a constant weld speed, the average values of the length residual stresses will increase as 30% with an increase in the rotational speed of the tool. The reason for this is the increase in the heating rate in the welding area. Also, at a constant rotational speed, the hardness in the welding area and the resistance to plastic deformation will increase with an increase in the weld speed. As a result, the average values of longitudinal residual stresses will increase. ANOVA analysis for selected factorial is shown in Table 9.

The Model F-value of 31.10 implies the model is significant. There is only a 0.01% chance that an F-value this large could occur due to noise. P-values less than 0.05 indicate model terms are significant. In this case A, B, C, BC are significant model terms. Relation between parameters and their effects on residual stress at different frequencies is shown in Figures 21-23.

At the end of the work, in order to evaluate the accuracy of the results related to the residual stress, according to Figure 24, all the samples were subjected to

**TABLE 9.** ANOVA for selected factorial

| Source | Sum of Squares | df | Mean Square | F-value | p-value | |
|---|---|---|---|---|---|---|
| **Model** | 10382.59 | 10 | 1038.26 | 31.10 | < 0.0001 | **significant** |
| **A-Rotational speed** | 6616.96 | 2 | 3308.48 | 99.10 | < 0.0001 | |
| **B-Welding speed** | 738.74 | 2 | 369.37 | 11.06 | 0.0010 | |
| **C-Frequency** | 2267.19 | 2 | 1133.59 | 33.96 | < 0.0001 | |
| **BC** | 759.70 | 4 | 189.93 | 5.69 | 0.0048 | |
| **Residual** | 534.15 | 16 | 33.38 | | | |
| **Cor Total** | 10916.74 | 26 | | | | |

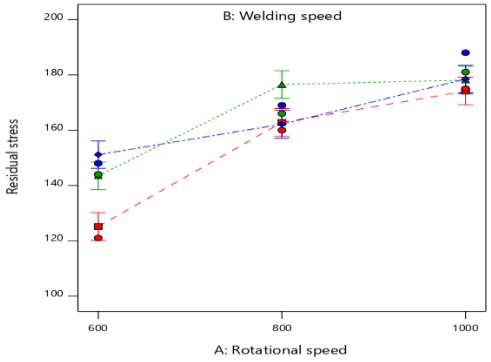


**Figure 21.** Relation between parameters at frequency 15KHz

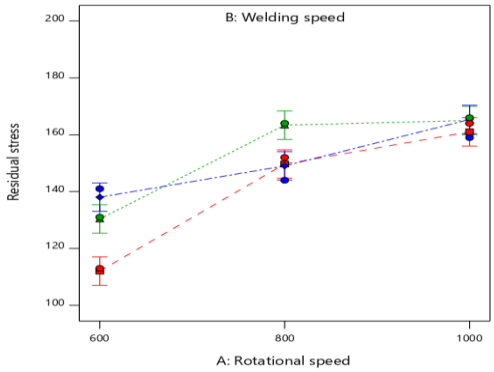


**Figure 22.** Relation between parameters at frequency 20KHz

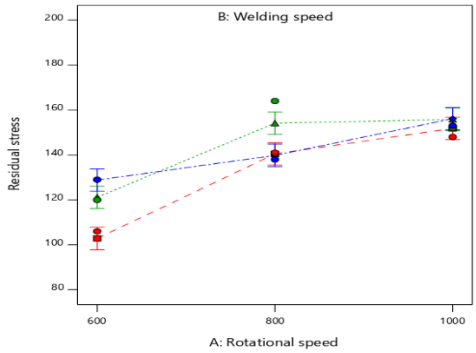


**Figure 23.** Relation between parameters at frequency 25KHz

**Figure 24.** Central drilling test with strain gauge installation

the central drilling test by installing a strain gauge, and it was found that the error is less than 10% and obtained results were accurate and appropriate.

## 4. CONCLUSION

According to the experiments, the results obtained from this research can be stated as follows:

- According to the results, it has been determined that at a constant weld speed, the average values of the length residual stresses will increase as average of 30% with an increase in the rotational speed of the tool.
- According to the investigations, it has been determined that at a constant weld speed, the hardness value in the stir area has decreased as average of 25% with an increase in the rotational speed of the tool, and its value will decrease by moving towards the two base metals.
- The strength and percentage of increase in length of ultrasonic friction stir welding samples are higher than their values in the case of friction stir welding samples as 15%.
- By increasing the rotational speed and decreasing the linear speed of the tool during the ultrasonic friction stir welding process, the grain size in the welding area increased and the strength values and percentage of length increase of the welded samples decreased.

- Ultrasonic vibrations will improve mechanical properties as 15% to 25% such as strength and residual stress in welded samples and these properties are directly related to each other.

## 5. REFERENCES


1. Yang, Q., Mironov, S., Sato, Y. and Okamoto, K., "Material flow during friction stir spot welding", ***Materials Science and Engineering: A***, Vol. 527, No. 16-17, (2010), 4389-4398. https://doi.org/10.1016/j.msea.2010.03.082
2. Eslami, S., Farahani, B.V., Tavares, P.J. and Moreira, P., "Fatigue behaviour evaluation of dissimilar polymer joints: Friction stir welded, single and double-rivets", ***International Journal of Fatigue***, Vol. 113, (2018), 351-358. https://doi.org/10.1016/j.ijfatigue.2018.04.024
3. Susmel, L., Hattingh, D.G., James, M.N. and Tovo, R.,, "Multiaxial fatigue assessment of friction stir welded tubular joints of al 6082-t6", ***International Journal of Fatigue***, Vol. 101, (2017), 282-296. https://doi.org/10.1016/j.ijfatigue.2016.08.010
4. Habibnia, M., Shakeri, M., Nourouzi, S. and Givi, M.B., "Microstructural and mechanical properties of friction stir welded 5050 al alloy and 304 stainless steel plates", ***The International Journal of Advanced Manufacturing Technology***, Vol. 76, (2015), 819-829. https://doi.org/10.1016/j.ijfatigue.2016.08.010
5. Boonchouytan, W., Chatthong, J., Rawangwong, S. and Burapa, R., "Effect of heat treatment t6 on the friction stir welded ssm 6061 aluminum alloys", ***Energy Procedia***, Vol. 56, (2014), 172-180. https://doi.org/10.1016/j.egypro.2014.07.146
6. Liu, H.-J., Zhang, H.-j., Huang, Y.-x. and Lei, Y., "Mechanical properties of underwater friction stir welded 2219 aluminum alloy", ***Transactions of Nonferrous Metals Society of China***, Vol. 20, No. 8, (2010), 1387-1391. https://doi.org/10.1016/S1003-6326(09)60309-5
7. El-Sayed, M., Shash, A. and Abd-Rabou, M., "Finite element modeling of aluminum alloy aa5083-o friction stir welding process", ***Journal of Materials Processing Technology***, Vol. 252, (2018), 13-24. https://doi.org/10.1016/j.jmatprotec.2017.09.008
8. Li, H., Gao, J. and Li, Q., "Fatigue of friction stir welded aluminum alloy joints: A review", ***Applied Sciences***, Vol. 8, No. 12, (2018), 2626. https://doi.org/10.1016/j.jmatprotec.2017.09.008
9. Thomä, M., Gester, A., Wagner, G., Straß, B., Wolter, B., Benfer, S., Gowda, D.K. and Fürbeth, W., "Application of the hybrid process ultrasound enhanced friction stir welding on dissimilar aluminum/dual-phase steel and aluminum/magnesium joints", ***Materialwissenschaft und Werkstofftechnik***, Vol. 50, No. 8, (2019), 893-912. https://doi.org/10.1002/mawe.201900028
10. Benfer, S., Straß, B., Wagner, G. and Fürbeth, W., "Manufacturing and corrosion properties of ultrasound supported friction stir welded al/mg-hybrid joints", ***Surface and Interface Analysis***, Vol. 48, No. 8, (2016), 843-852. https://doi.org/10.1002/sia.5871
11. Thomä, M., Wagner, G., Straß, B., Wolter, B., Benfer, S. and Fürbeth, W., "Ultrasound enhanced friction stir welding (use-fsw) of hybrid aluminum/steel joints", in Friction Stir Welding and Processing X, Springer. (2019), 23-32.
12. Hong, K., Wang, Y., Zhou, J., Zhou, C. and Wang, L., "Investigation on ultrasonic assisted friction stir welding of aluminum/steel dissimilar alloys", ***High Temperature Materials and Processes***, Vol. 40, No. 1, (2021), 45-52. https://doi.org/10.1515/htmp-2021-0011
13. El-Morsy, A.-W., Ghanem, M.M. and Bahaitham, H., "Effect of friction stir welding parameters on the microstructure and mechanical properties of aa2024-t4 aluminum alloy", ***Engineering, Technology & Applied Science Research***, Vol. 8, No. 1, (2018). https://doi.org/10.48084/etasr.1704
14. Shukla, S., Komarasamy, M. and Mishra, R.S., "Grain size dependence of fatigue properties of friction stir processed ultrafine-grained al-5024 alloy", ***International Journal of Fatigue***, Vol. 109, (2018), 1-9. https://doi.org/10.1016/j.ijfatigue.2017.12.007
15. Peng, Y., Zhao, J., Chen, L.-s. and Dong, J., "Residual stress measurement combining blind-hole drilling and digital image correlation approach", ***Journal of Constructional Steel Research***, Vol. 176, (2021), 106346. https://doi.org/10.1016/j.jcsr.2020.106346
16. Sutton, M.A., Wolters, W., Peters, W., Ranson, W. and McNeill, S., "Determination of displacements using an improved digital correlation method", ***Image and Vision Computing***, Vol. 1, No. 3, (1983), 133-139. https://doi.org/10.1016/0262-8856(83)90064-1
17. Niezrecki, C., Baqersad, J. and Sabato, A., "Digital image correlation techniques for non-destructive evaluation and structural health monitoring", ***Handbook of Advanced non-Destructive Evaluation***, (2018), 46. https://doi.org/10.1007/978-3-319-26553-7_47
18. Schajer, G. and Yang, L., "Residual-stress measurement in orthotropic materials using the hole-drilling method", ***Experimental Mechanics***, Vol. 34, (1994), 324-333. https://doi.org/10.1007/BF02325147
19. Shokrieh, M.M. and Ghasemi K, A.R., "Determination of calibration factors of the hole drilling method for orthotropic composites using an exact solution", ***Journal of Composite Materials***, Vol. 41, No. 19, (2007), 2293-2311. https://doi.org/10.1177/0021998307075443
20. Standard, A., "E837-08 standard test method for determining residual stresses by the hole-drilling strain-gage method", ASMT International, West Conshohocken, PA, (2008). https://doi.org/10.1520/e0837-01
21. Khanjanzadeh, P., Amirabadi, H. and Sadri, J., "Design of broaching tool using finite element method for achieving the lowest residual tensile stress in machining of ti6al4v alloy", ***International Journal of Engineering, Transactions A: Basics***, Vol. 33, No. 4, (2020), 657-667. doi: 10.5829/IJE.2020.33.04A.17.
22. Khanjanzadeh, P., Amirabadi, H. and Sadri, J., "Experimental study on surface integrity of ti6al4v by broaching", ***International Journal of Engineering, Transactions B: Applications***, Vol. 35, No. 2, (2022), 481-492. doi: 10.5829/IJE.2022.35.02B.24.

## Persian Abstract

**چکیده**

در این پژوهش به بررسی اتصال آلیاژ آلومینیوم ۵۰۵۲ به فولاد زنگ نزن آستنیتی ۳۰٤ پرداخته شده است. بدین منظور از فرآیند جوشکاری اصطکاکی اغتشاشی در دو حالت به همراه ارتعاشات فراصوتی و ساده استفاده شده است. به منظور دستیابی به بهترین کیفیت جوش از لحاظ خواص مکانیکی و متالورژیکی، پارامترهای جوشکاری نظیر سرعت دورانی، سرعت خطی و فرکانس مورد بررسی قرار گرفته است. هدف این تحقیق دستیابی به بهترین خواص مکانیکی و متالورژیکی با کمترین تنش پسماند در نمونه غیرهمجنس جوشکاری شده است. با هدف اندازه‌گیری مقادیر تنش پسماند ایجاد شده در نمونه‌ها پس از انجام عملیات جوشکاری از روش نوین سوراخکاری-برهمنگاری تصاویر دیجیتالی استفاده شده است. در انتها با بررسی نتایج مشخص شده است که ارتعاشات فراصوتی سبب بهبود خواص مکانیکی تا حدود ۱۵٪ و خواص متالورژیکی را هم تا حد زیادی بهبود داده است. به منظور بررسی صحت نتایج مربوط به تنش پسماند، تمامی نمونه ها با نصب کرنش سنج به روش سوراخکاری مرکزی تحت آزمایش قرار گرفتند و مشخص شد که خطای کمتر از ۱۰ درصد بوده و نتایج به دست آمده مناسب و قابل قبول بوده است.